Korea-Australia Rheology Journal
Vol. 15, No. 2, June 2003 pp. 75-82

Deformation of multiple non-Newtonian drops in the entrance region

See Jo Kim*, Sang Dae Kim and Youngdon Kwon[1]
Department of Mechanical Engineering, Andong National University, Kyungbuk 60-749, Korea
[1]Textile Engineering, Sungkyunkwan University, Suwon, Kyonggi 440-746, Korea
(Received March 18, 2003; final revision received May 9, 2003)

Abstract

In this study, with the finite element method we numerically investigate the deformation of liquid drops surrounded by Newtonian or non-Newtonian viscous medium in the axisymmetric contraction flow. 1, 2 or 4 Newtonian or non-Newtonian drops are considered and the truncated power-law model is applied in order to describe non-Newtonian viscous behavior for both fluids. In this type of flow the drop exhibits considerably large deformation, and thus techniques of unstructured mesh generation and auto-remeshing are employed to accurately express the fluid mechanical behavior. We examine the deformation pattern of liquid drops with viscosity dependence different from that of the surrounding medium and also explain their interactions by comparing relative position or speed of drop front.

Keywords **:** drop deformation, auto-remeshing, power-law liquid, surface tension, contraction flow, multiphase flow

1. Introduction

It is quite meaningful in engineering aspect to investigate liquid drop behavior in two-phase flow, on which flow mixing or overall rheological characteristics heavily depend. When two immiscible fluids are mixed, one discrete phase (liquid drops) surrounded by another continuous phase is usually formed and it continuously deforms under the flow. Thus behavior of the drops determines in part mixing characteristics and eventually mechanical properties of the final product.

During the past three decades, one can observe swift progress made in this field of study. Since the experimental and theoretical study on drop deformation by Taylor (1934), Hyman and Skalak (1972) have calculated axisymmetric small deformation of Newtonian drops immersed in another Newtonian liquid moving along the centerline of the cylindrical tube. Bozzi *et al.* (1997) have employed a finite element method to describe axisymmetric steady deformation of Newtonian drops suspended in Newtonian liquid along a vertical tube under gravity. A study on deformation of a non-Newtonian drop in another non-Newtonian liquid employing the finite element method has been recently reported (Kim and Han, 2001).

In this study, we describe the shape of deforming liquid drops immersed in fluid flowing through an axisymmetric contraction tube. The drops and the surrounding liquid are considered to be Newtonian/Newtonian, non-Newtonian/Newtonian or non-Newtonian/non-Newtonian. In order to express non-Newtonian viscosity behavior, the truncated power-law model is applied. Employing the penalty function method, we remove the pressure variable from the governing equations and thus computational efficiency is enhanced. Auto remeshing as well as unstructured mesh generation is implemented to appropriately express continuous and large deformation of moving drops (Kim, 2000).

2. Theory

Since the numerical algorithm employed in this study including the unstructured mesh generation and auto-remeshing has been explained in previous works, it is not described here again. Detailed description of the computational algorithm can be found in papers (Kim, 2000; Kim and Han, 2001) and cited references.

2.1. Continuity and momentum equations

The continuity and momentum equations for the drop and surrounding liquid are

$$\nabla\cdot\boldsymbol{v}_m = 0; \qquad \nabla\cdot\boldsymbol{v}_d = 0, \tag{1}$$

$$\rho_m\left(\frac{\partial \boldsymbol{v}_m}{\partial t}+\boldsymbol{v}_m\cdot\nabla\boldsymbol{v}_m\right) = -\nabla p_m+\nabla\cdot\boldsymbol{\tau}_m;$$

$$\rho_d\left(\frac{\partial \boldsymbol{v}_d}{\partial t}+\boldsymbol{v}_d\cdot\nabla\boldsymbol{v}_d\right) = -\nabla p_d+\nabla\cdot\boldsymbol{\tau}_d. \tag{2}$$

*Corresponding author: sjkim1@andong.ac.kr
© 2003 by The Korean Society of Rheology

Here v is the velocity, p the pressure, ρ the liquid density, τ the extra stress tensor, ∇ the gradient operator, and subscripts m and d designate surrounding medium and drop, respectively.

2.2. Truncated power-law model

The non-Newtonian viscosity $\mu(\dot{\gamma})$ of immiscible liquids is expressed by the following truncated power-law model, which assigns constant viscosity for deformation gradient $\dot{\gamma}$ lower than $\dot{\gamma}_{mc}$ or $\dot{\gamma}_{dc}$ but exhibits power-law type dependence of viscosity on $\dot{\gamma}$ higher than that:

i) Viscosity of surrounding liquid

$$\mu(\dot{\gamma}) = \begin{cases} \mu_{m0} & \text{for } \dot{\gamma} \le \dot{\gamma}_{mc} \\ K_m \dot{\gamma}^{n_m - 1} & \text{for } \dot{\gamma} \le \dot{\gamma}_{mc} \end{cases} \tag{3}$$

ii) Viscosity of drops

$$\mu(\dot{\gamma}) = \begin{cases} \mu_{d0} & \text{for } \dot{\gamma} \le \dot{\gamma}_{dc} \\ K_d \dot{\gamma}^{n_d - 1} & \text{for } \dot{\gamma} \le \dot{\gamma}_{dc} \end{cases} \tag{4}$$

Here subscripts m and d again denote surrounding medium and drops. μ_{m0} and μ_{d0} are zero shear viscosities, $\dot{\gamma}_{mc}$ and $\dot{\gamma}_{dc}$ critical shear rates, K_m and K_d consistency indices, and n_m and n_d are power-law indices of liquid medium and drop, respectively. The magnitude of deformation gradient, $\dot{\gamma}$ is defined to be

$$\dot{\gamma} = \sqrt{2 D_{ij} D_{ij}}, \tag{5}$$

where D_{ij} is the strain rate tensor.

2.3. Interfacial tension

At the interface between the surrounding medium and liquid drops the condition of interfacial force balance has to be satisfied. It can be expressed as the relation between interface curvature and total stress difference in the following:

$$\boldsymbol{nn}:(\boldsymbol{T}_m - \boldsymbol{T}_d) = \frac{\xi}{\boldsymbol{R}_c}, \tag{6}$$

$$\boldsymbol{tn}:(\boldsymbol{T}_m - \boldsymbol{T}_d) = 0. \tag{7}$$

Here ξ is the interfacial tension, $\boldsymbol{R}_c$ the radius of interface curvature, $\boldsymbol{t}$ and $\boldsymbol{n}$ are unit tangent and outward unit normal vectors on the interface, respectively, and $\boldsymbol{T}_m$ and $\boldsymbol{T}_d$ are total stress tensors of medium and drop. The radius of curvature in this axisymmetric polar coordinate (r,z) is computed by the following:

$$\frac{1}{R_c} = \left[\frac{d\boldsymbol{t}}{ds} \cdot \boldsymbol{n} + \frac{1}{r}\frac{dz}{ds} \right] \tag{8}$$

where s is the arc length along the interface measured from the forward stagnation point. In the numerical calculation performed herein, the interfacial tension ξ is assumed constant and specified as 0.01.

2.4. Boundary conditions

Fig. 1 illustrates computational domain, geometry and boundary conditions considered in this work. We have assumed that during flow two liquids are incompressible and completely immiscible. The liquid drops are neutrally buoyant and thus they move along the centerline of the tube. The inlet and outlet boundaries are assigned the fully developed velocity profiles and no-slip wall boundary is also applied. SI unit system is employed for all the measure. The radius of spherical drops R_d is 0.0015(m), the radii of inlet and outlet of the tube are 0.012(m) and 0.003(m), respectively. Thus the standard 4:1 contraction geometry is considered. For comparison, 1, 2 or 4 liquid drops are placed on the centerline of the tube. The lengths of inlet and outlet tubes are set as 0.03(m) and 0.06(m), respectively. The critical shear rate $\dot{\gamma}_{mc}$ or $\dot{\gamma}_{dc}$ for both fluids is specified as 0.1(s^{-1}) and the volumetric flow rate Q in all computations is assigned as 2.12×10^{-7}(m^3/s).

3. Computation results and discussion

Detailed description of the convergence of the finite-element analysis of the present two-phase simulation can be found in papers (Kim, 2000; Kim and Han, 2001), in which several finite element meshes were tested. The initial finite-element meshes for 1, 2, and 4 drops are shown in Fig. 2, respectively. At each time step, a modified

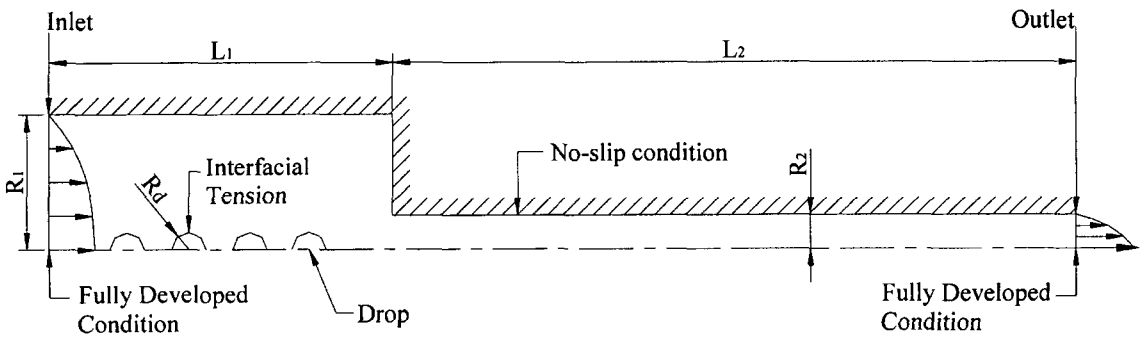

Fig. 1. Schematic diagram describing the flow geometry and boundary conditions.

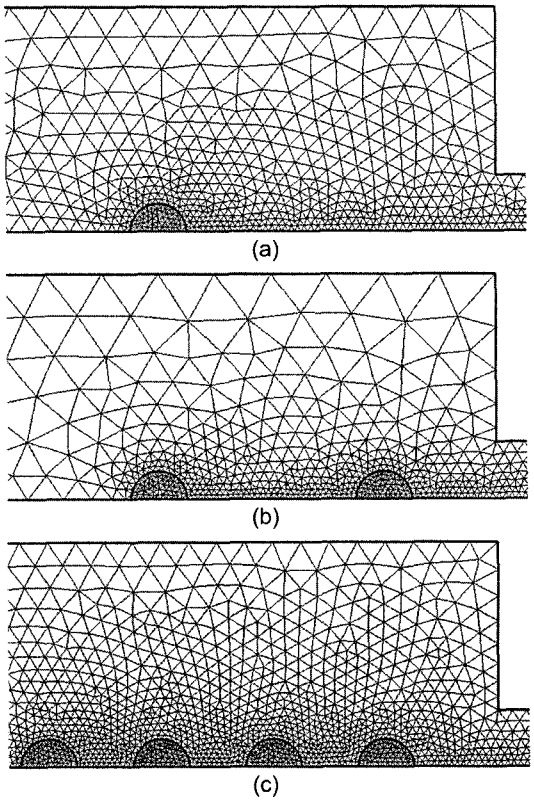

Fig. 2. Three different initial finite element meshes for 1, 2, and 4 drops.

Newton-Raphson method was used as an iteration technique to deal with non-Newtonian materials(Kim and Kwon, 1995).

Figs. 3-5 show shape of deformed drops at the entrance of the tube contraction. Regardless of viscosity characteristics, tendency of drop deformation as a whole exhibits sharpening of moving fronts whereas rear parts maintain oval shape. In Fig. 3, deformation of a single drop at the entrance region is illustrated. Newtonian/Newtonian (a) and non-Newtonian/Newtonian (c) cases exhibit similar behavior due to little deviation of the non-Newtonian drop with the power-law index $n_d = 0.8$ from the Newtonian. However in the case of (d) $n_d = 0.4$, the drop displays significant shear thinning. Thus the moving front of the drop becomes very sharp in the beginning of entering the tube contraction and the drop is then extended to long elliptical shape. For non-Newtonian/non-Newtonian liquid mixture (b) with $n_d = 0.8$, the amount of drop deformation decreases. The similar trend of deformation for the leading drop in the case of 2 or 4 drops placed on the centerline of the tube may be observed in Figs. 4 and 5.

In order to explain different deformation behavior as described above, let us consider the effects of viscosity ratio ($\lambda = \mu_d/\mu_m$) of liquid mixtures in Fig. 3. The ratios are 10, 10, 3.9, and 0.6, respectively, when $\dot{\gamma} = 100.0\ s^{-1}$ is applied as a flow field. As pointed out by Kim and Han

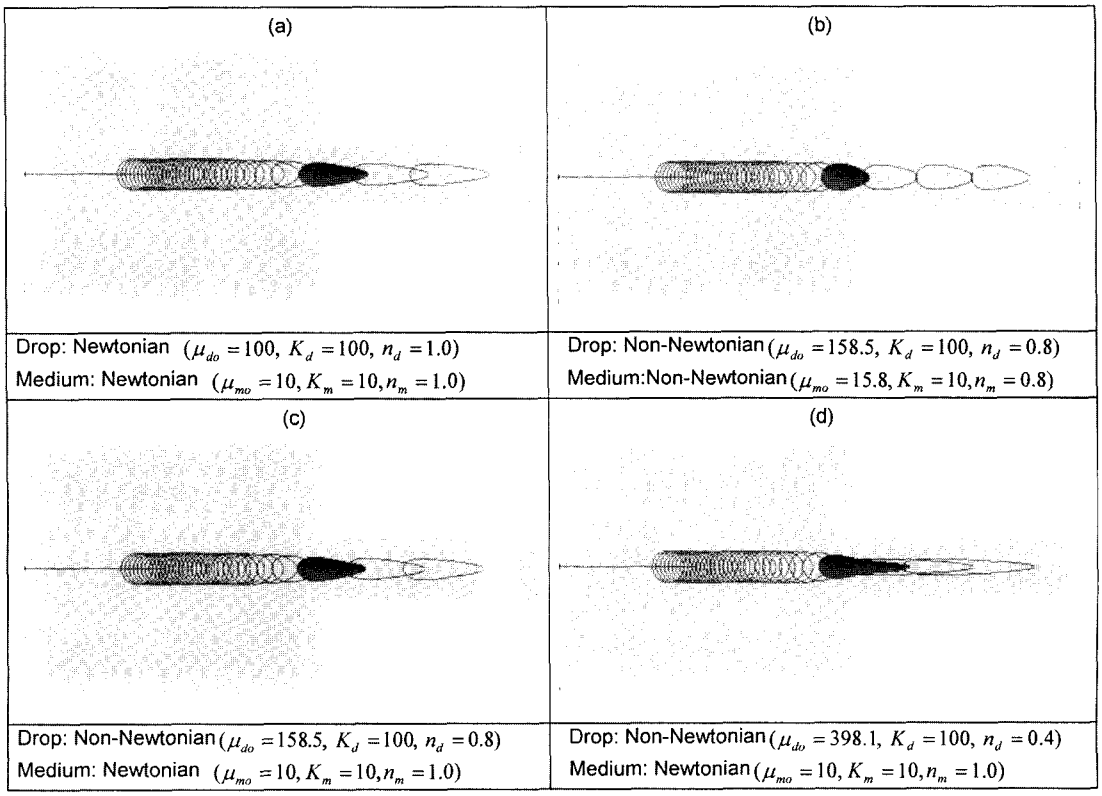

Fig. 3. Computed shapes of a drop for four different liquid mixtures.

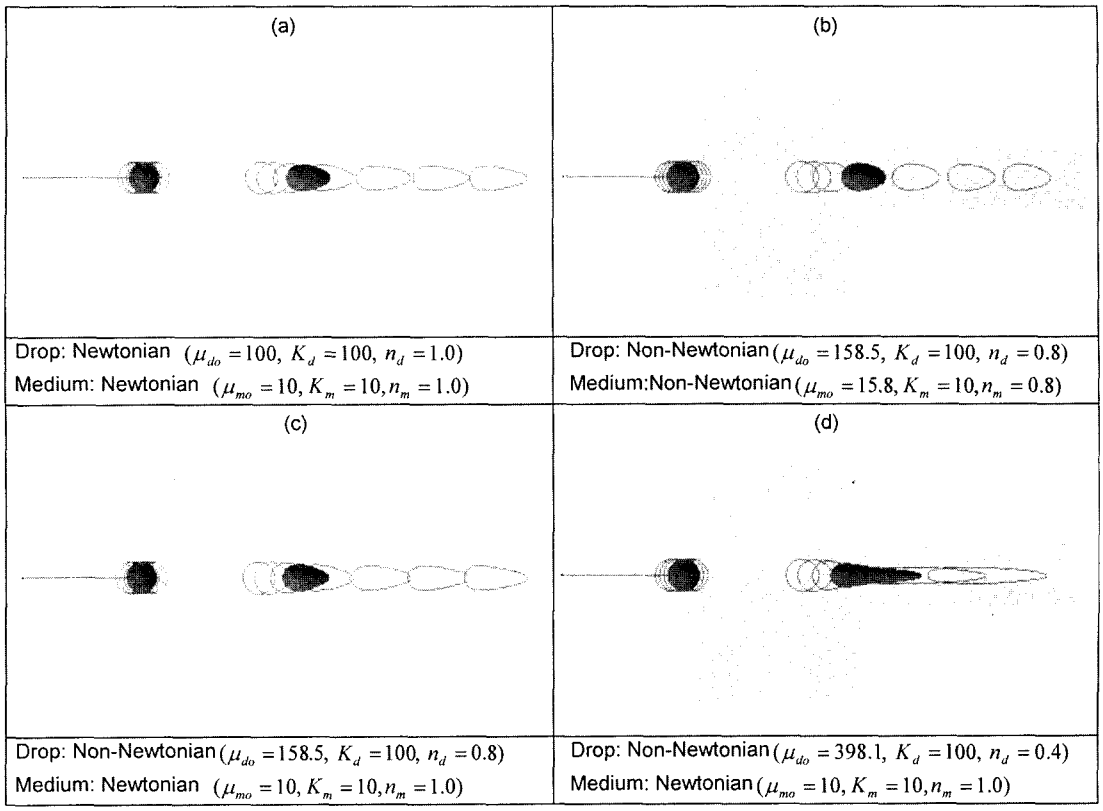

Fig. 4. Computed shapes of two drops for four different liquid mixtures.

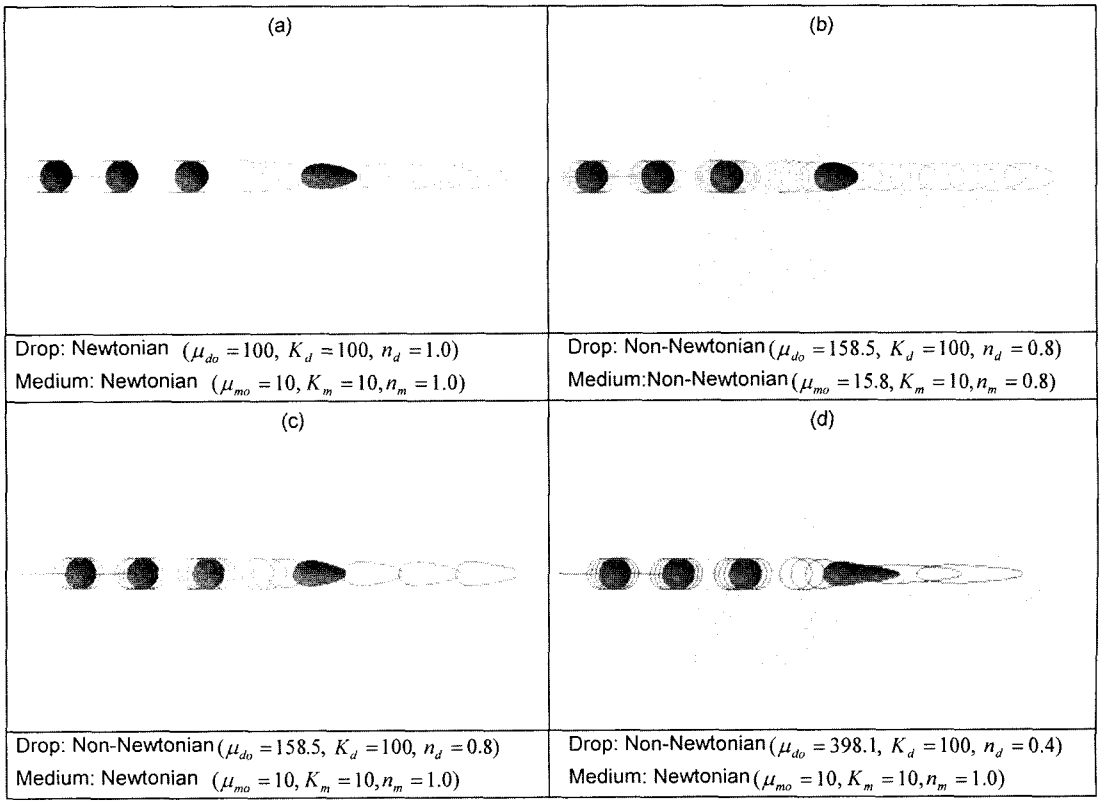

Fig. 5. Computed shapes of four drops for four different liquid mixtures.

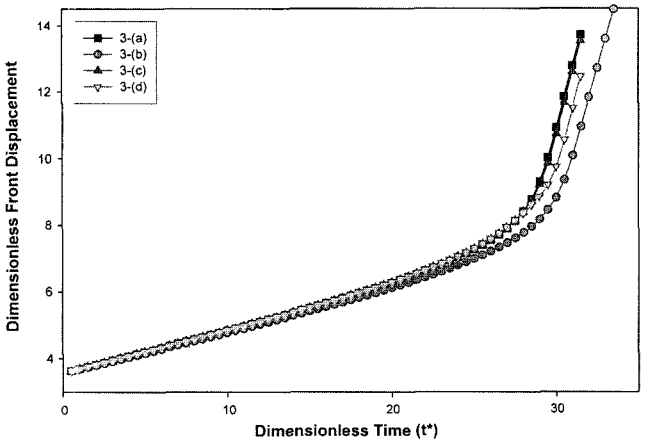

Fig. 6. Plot of dimensionless displacement vs. dimensionless time of the drop front in the case of a single drop suspending in the medium.

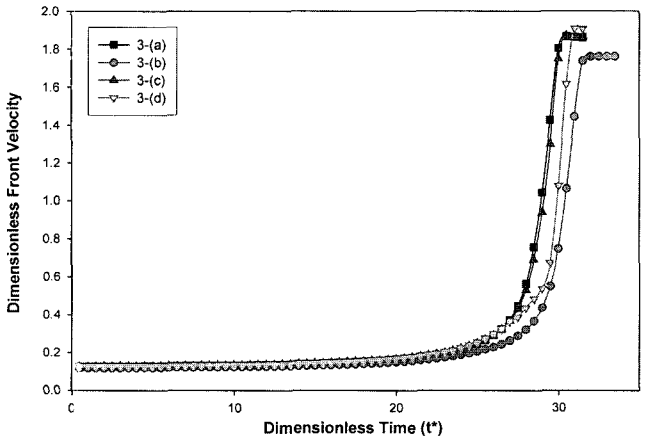

Fig. 7. Plot of dimensionless velocity vs. dimensionless time of the drop front in the case of a single drop suspending in the medium.

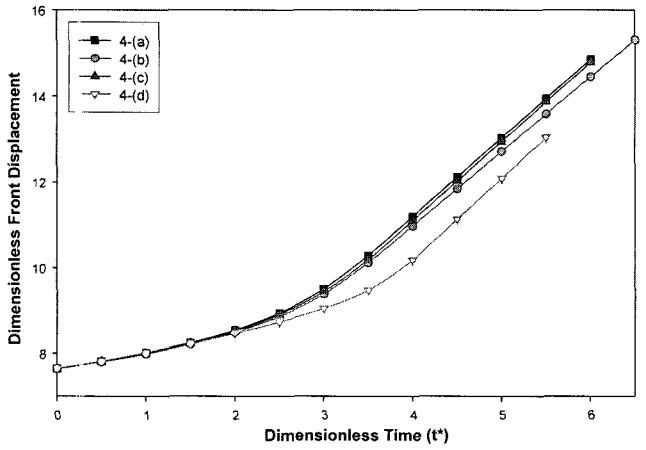

Fig. 8. Plot of dimensionless displacement vs. dimensionless time of the leading drop front in the case of 2 drops suspending in the medium.

(2001), the extent of drop deformation increases dramatically as the viscosity ratio decreases (i.e., as the viscosity of the suspending medium is raised or the viscosity of drop is reduced). Therefore, this explains why the drop in the case of Fig. 3(d) exhibits the largest deformation in comparison with those of (a), (b) and (c).

Figs. 6-15 explain time evolutions of front displacement and velocity of the leading or the second drops for each case of Figs. 3-5. All the dependence is expressed according to the dimensionless time(t^*), velocity (v^*), and displacement(l^*) variables defined as

$$t^* = \frac{t}{(R_2/u_0)}, \quad v^* = \frac{v}{(v_0)}, \quad l^* = \frac{l}{(R_2)} \tag{9}$$

where $u_0 = Q/(\pi R_2^2)$ is the average fluid velocity. Dimensionless displacements of the leading drop front are depicted in Figs. 6, 8 and 12 for a single drop, 2 and 4 drops, respectively. In all the cases, the liquid mixture of (a) Newtonian/Newtonian exhibits almost the same behavior with the mixture of (c) non-Newtonian($n_d = 0.8$)/Newtonian possibly due to negligible shear thinning effect of the non-Newtonian drops. Examining the results for (b) and (d), we find that the drop front of (d) non-Newtonian($n_d = 0.4$)/Newtonian liquid advances faster than that of (b) non-Newtonian($n_d = 0.8$)/non-Newtonian($n_d = 0.8$) for a single drop placed in the tube. With the same flow rate velocity of Newtonian medium at the tube center is higher than that of non-Newtonian medium, which effects on the velocity of the leading drop. This is the main reason to these results. However this situation is reversed for the other cases, that is, when 2 or 4 drops are located in a row, the front of the leading drop in the non-Newtonian medium moves faster than that in the Newtonian liquid. Even though it is difficult to explain the reason mentioned above it is easily seen that this effect of the inserted multiple drop on the displacement or velocity of the leading drop is higher in the non-Newtonian fluid system than in the Newtonian fluid system.

In Figs. 7, 9 and 13, the leading drop fronts show dramatic increase of the velocity near the entrance to tube contraction and then they reach steady speed once the leading drop completely gets inside the narrow tube. Again the cases of (a) and (c) exhibit similar behavior, but those of (b) and (d) demonstrate dependence of front speed on the number of drops present in the flow domain. In the case of a single drop shown in Fig. 7, the speed for (d) lies between (a) (or c) and (b) when the drop passes through the contraction, but it reaches the highest steady value inside the narrow tube. On the other hand, in Fig. 9 when 2 drops are located on the centerline, the front speed of the leading drop for (d) manifests the lowest gain of speed near the entrance region, but the speed for (b) shows evolution pattern similar to (a) and (c) with slightly lower steady value. Fig. 13 explains behavior of the front speed for 4

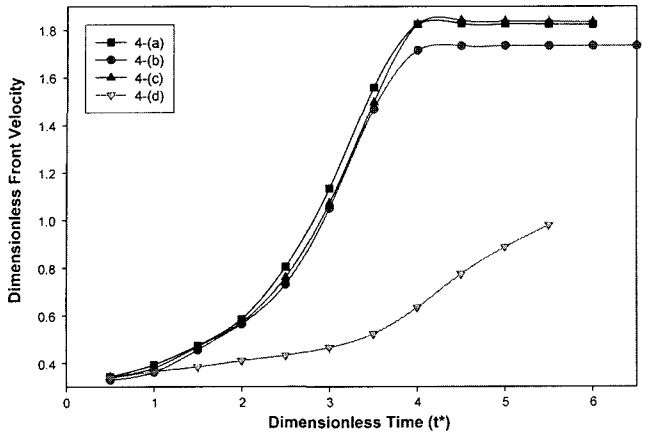

Fig. 9. Plot of dimensionless velocity vs. dimensionless time of the leading drop front in the case of 2 drops suspending in the medium.

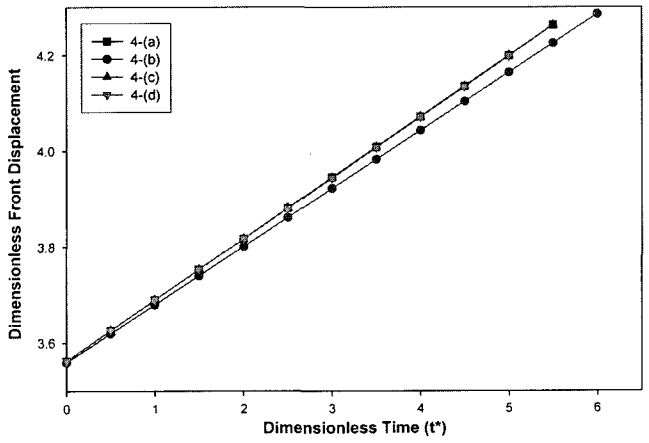

Fig. 10. Plot of dimensionless displacement vs. dimensionless time of the second drop front in the case of 2 drops suspending in the medium.

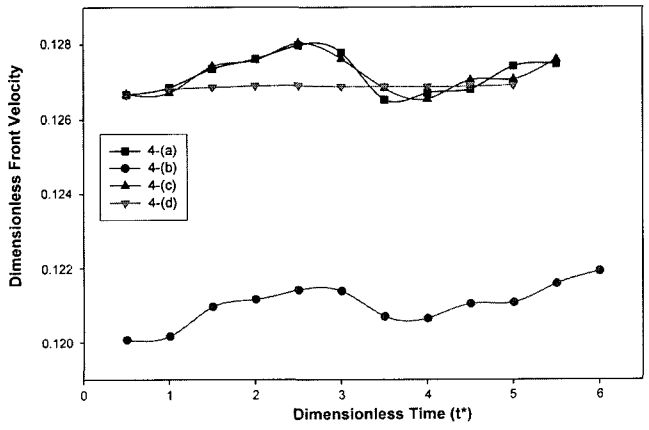

Fig. 11. Plot of dimensionless velocity vs. dimensionless time of the second drop front in the case of 2 drops suspending in the medium.

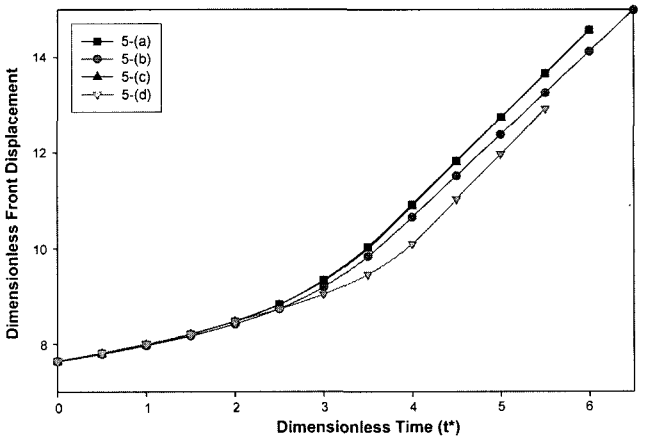

Fig. 12. Plot of dimensionless displacement vs. dimensionless time of the leading drop front in the case of 4 drops suspending in the medium.

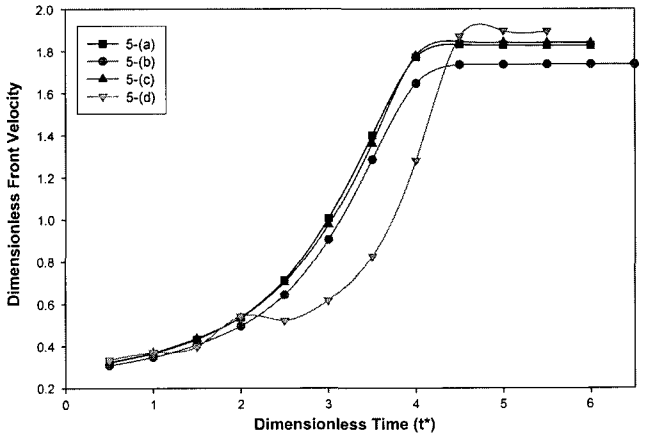

Fig. 13. Plot of dimensionless velocity vs. dimensionless time of the leading drop front in the case of 4 drops suspending in the medium.

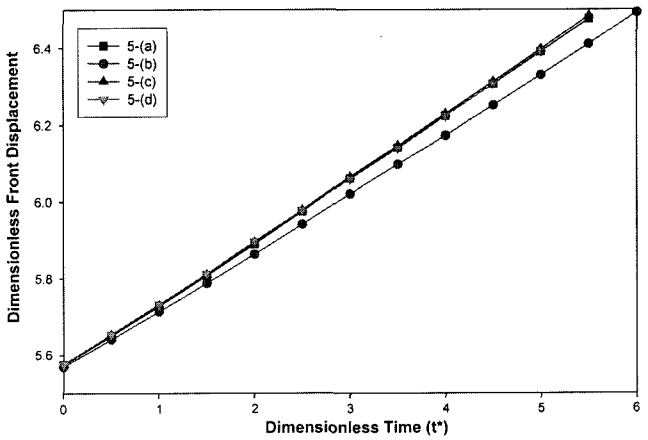

Fig. 14. Plot of dimensionless displacement vs. dimensionless time of the second drop front in the case of 4 drops suspending in the medium.

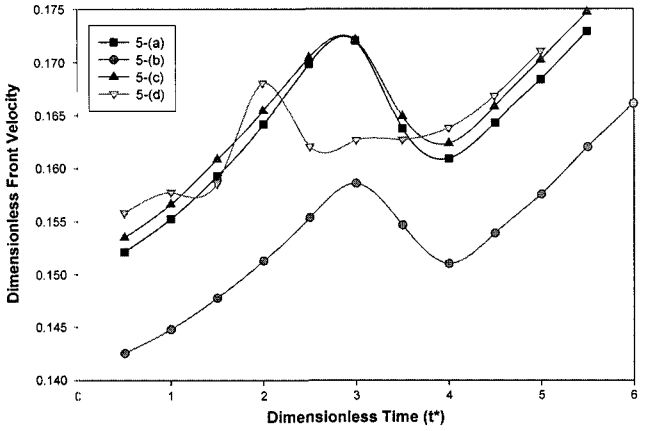

Fig. 15. Plot of dimensionless velocity vs. dimensionless time of the second drop front in the case of 4 drops suspending in the medium.

drops suspended in flow domain. Although the time evolution of the drop speed for three cases of (a), (b) and (c) looks quite similar to that for respective cases in Fig. 9, the speed of (d) exhibits slight oscillation before contraction and then dramatic increase to the highest steady value. All the above results demonstrate typical complication in detailed behavior of 2-phase flow that prevents intuitive prediction of multi-phase flow characteristics, especially when multiple drop interaction has to be taken into consideration.

Figs. 10 and 14 illustrate time evolution of displacements for the front of the second drop following the leading one. All combination of immiscible liquids except the one for (b) shows almost identical dependence on time, but the second drop front of (b) advances relatively slowly. In Figs. 11 and 15. their speed variation is expressed. Even though the absolute value of speed variation is small, its dependence for (a), (b) and (c) shows quite similar tendency: the speed increases in the beginning ($0<t^*<3$), then decreases to a minimum when the leading drop reaches the steady speed, and afterwards increases again. Among those 3 types of liquid mixture, the case of (b) corresponds to the slowest speed irrespective of its similar variation. On the other hand, the second non-Newtonian drop in the Newtonian medium moves forward at almost constant speed for the case of 2 drops ((d) of Fig. 11), but it demonstrates some peculiar evolution of speed in the case of 4 drops present. Again these results suggest possible extreme difficulty in predicting multi-phase flow behavior for non-Newtonian liquid mixtures. Also all the above consequences may vary if the spacing between adjacent drops changes and if the viscosity ratio changes.

4. Conclusion

Employing the finite element method, we numerically investigate the drop deformation in the axisymmetric 4:1 contraction flow when the immiscible dispersed phase and the surrounding medium are either Newtonian or non-Newtonian fluid. In order to describe non-Newtonian shear thinning behavior of the viscous liquid, the truncated power-law model is applied. We examine the flow behavior with 1, 2 or 4 drops suspending in the medium to study mutual hydrodynamic interaction among drops during the contraction flow. In general, the lower the power-law index for the drop becomes, the more severely the front drop deforms with sharp front and oval rear parts, as it enters the contraction region with or without following drops. For quantitative comparison of effects exerted by multiple drops, we have also investigated in depth the time evolution of displacements and speeds of drop fronts. Certainly in all the cases of various liquid mixtures, the speed of the leading drop front first increases near the contraction tube entrance, and then it reaches a steady value once the drop completely gets inside the downstream tube. The detailed behavior of drop deformation or speed varies significantly according to the existence of the hydrodynamic interaction among drops. It seems that more extensive experimental as well as theoretical study is required to explain complicated deformation behavior exhibited by hydrodynamic interactions of multiple drops. However in this work, we have tried to explain various flow behaviors according to viscosity ratio, power-law index and the number of drops. By means of the numerical approach employed herein, it is clearly demonstrated that the presence of multiple drops suspended in the medium alters the flow pattern quite significantly. Consequently the current numerical scheme provides evidence of complexity involved in multi-phase non-Newtonian flow, which prohibits easy and intuitive prediction of flow characteristics and thus makes the numerical study more valuable.

Acknowledgement

This work was supported by grant No. R02-2001-000-01215-0 from the Basic Research Program of the Korea Science & Engineering Foundation.

References

Bozzi, E. B., J. Q. Feng, T. C. Scott and A. J. Pearlstein, 1997, Steady axisymmetric motion of deformable drops falling or rising through a homogeneous fluid in a tube at intermediate Reynolds number, *J. Fluid Mech.* **336**, 1-32.

Hyman, W. A. and R. Skalak, 1972, Non-Newtonian behavior of a suspension of liquid drops in tube flow, *AIChE J.* **18**, 149-154.

Kim, S. J., 2000, Development of a finite element method with auto-remeshing techniques for analysis of the droplet deformation in a two-phase polymeric mixture, *J. Korean Fiber Soc.* **37**, 234-241.

Kim, S. J. and C. D. Han, 2001, Finite element analysis of axisymmetric creeping motion of a deformable non-Newtonian drop in the entrance region of a cylindrical tube, *J. Rheol.* **45**, 1279-1303.

Kim, S. J. and T. H. Kwon, 1995, Development of numerical simulation methods and analysis of extrusion processes of particle-filled plastic materials subject to slip at the wall, *Powder Technol.* **85**, 227-239.

Taylor, G. I., 1934, The formation of emulsion in definable fields of flow, *Proc. R. Soc. London* **A146**, 501-523.